Available online at www.sciencedirect.com
SCIENCE DIRECT®
Icarus 183 (2006) 168–178
ICARUS
www.elsevier.com/locate/icarus

The color of the Kuiper belt Core

Amanda A.S. Gulbis [a,*], J.L. Elliot [a,b,c], Julia F. Kane [a]

[a] Department of Earth, Atmospheric, and Planetary Sciences, Massachusetts Institute of Technology, Cambridge, MA 02139, USA
[b] Department of Physics, Massachusetts Institute of Technology, Cambridge, MA 02139, USA
[c] Lowell Observatory, 1400 W. Mars Hill Rd., Flagstaff, AZ 86001, USA

Received 29 October 2004; revised 23 January 2006

Available online 24 March 2006

Abstract

Recent dynamical analyses of the Kuiper belt have introduced a rigorous classification scheme, determined the mean orbital plane, and identified "Core" and "Halo" populations as a function of inclination with respect to this plane (Elliot, J.L., Kern, S.D., Clancy, K.B., Gulbis, A.A.S., Millis, R.L., Buie, M.W., Wasserman, L.H., Chiang, E.I., Jordan, A.B., Trilling, D.E., Meech, K.J., 2005. Astron. J. 129, 1117–1162). Here, we use new observations and existing data to investigate the colors of Kuiper belt objects (KBOs) within this framework. With respect to the bulk KBO color distribution (all objects for which we have $B–V$ and $V–R$ colors; median $B–R = 1.56$), we find that the population of objects classified following (Elliot, J.L., Kern, S.D., Clancy, K.B., Gulbis, A.A.S., Millis, R.L., Buie, M.W., Wasserman, L.H., Chiang, E.I., Jordan, A.B., Trilling, D.E., Meech, K.J., 2005. Astron. J. 129, 1117–1162) as Classical tends to be red ($B–R > 1.56$) while the Scattered Near population is mostly neutral ($B–R < 1.56$). Colors of Scattered Extended and Resonant objects are consistent with the bulk distribution. Separating objects into specific resonances demonstrates that the color of the Resonant sample is dominated by KBOs in the 3:2 resonance, which is consistent with previous findings. Unlike the objects in the 3:2 resonance, however, the majority of objects in the 5:2 resonance are neutral and all but one of the objects in the 4:3, 5:3, 7:4, 2:1, and 7:3 resonances are red. In particular, the objects in the 7:4 resonance are remarkably red. We find that the colors of KBOs in the Core (low-inclination) and Halo (high-inclination) are statistically different, with Core objects being primarily red and Halo objects having a slight tendency to be neutral. Notably, virtually all of the non-Resonant Core objects are red. This combination of low inclination, unperturbed orbits and red colors in the Core may be indicative of a relic grouping of objects.
© 2006 Elsevier Inc. All rights reserved.

Keywords: Kuiper belt objects; Photometry

1. Introduction

First theorized over half a century ago (Leonard, 1930; Edgeworth, 1949; Kuiper, 1951), the existence of a population of objects other than Pluto and Charon beyond the orbit of Neptune was not observationally established until 1992 (Jewitt and Luu, 1993). More than one thousand bodies (http://cfa-www.harvard.edu/iau/lists/MPLists.html) have since been discovered in what is now known as the Kuiper belt. Because Kuiper belt objects (KBOs) are considered remnants of the protoplanetary disk, studies of these bodies increase our understanding of the formation and evolution of the outer Solar System. Grouping KBOs dynamically, or by their physical properties, is a way to gain insight into the history of the region.

Traditionally, KBOs have been divided into classes based on their orbital elements: "resonant," objects in a dynamical resonance with Neptune; "classical," non-Resonant objects that have low inclination and/or eccentricity; and "scattered," non-Resonant objects with high inclination and/or eccentricity. While the designation "classical" could be interpreted as a grouping of primitive objects, it is a fairly general term that has been inconsistently defined within the community. In particular, the boundary between "classical" and "scattered" is somewhat arbitrary (Elliot et al., 2005). An alternative method of distinguishing objects is by their physical characteristics, through surface color measurements. Several groups have made photometric measurements of KBOs, and the visible color distribution ranges from neutral (solar-like) to extremely

* Corresponding author. Fax: +1 617 253 2886.
E-mail address: gulbis@mit.edu (A.A.S. Gulbis).

0019-1035/$ – see front matter © 2006 Elsevier Inc. All rights reserved.
doi:10.1016/j.icarus.2006.01.021

red (e.g., Green et al., 1997; Tegler and Romanishin, 2000; Jewitt and Luu, 2001; Boehnhardt et al., 2001; Doressoundiram et al., 2002; Tegler et al., 2003; Peixinho et al., 2004). The faintness of KBOs makes color observations difficult, resulting in small-number statistics and evolving interpretations of the data. A prime example is the reported existence of two, distinctly colored, groups of KBOs (Tegler and Romanishin, 1998; Tegler and Romanishin, 2000; Tegler and Romanishin, 2003) that has been drawn into question (Jewitt and Luu, 2001; Barucci et al., 2001; Peixinho et al., 2003). Nonetheless, color patterns have emerged. Those patterns with particular relevance to this work are that objects on nearly circular orbits with perihelion distances $q > 40$ AU have been shown to be systematically redder than the general population (Tegler and Romanishin, 2000; Jewitt and Luu, 2001; McBride et al., 2003), and a relationship between color and inclination has been reported within the sub-grouping of "classical" objects (Tegler and Romanishin, 2000; Trujillo and Brown, 2002; Doressoundiram et al., 2002; McBride et al., 2003; Tegler et al., 2003; Peixinho et al., 2004).

Recent work by Elliot et al. (2005) provides a rigorous scheme by which KBOs are classified. These classifications are based on the behavior of orbital integrations over 10 Myr. For each object, 107 different arguments are tested for libration, providing unprecedented information on the occupancy of resonances. Elliot et al. (2005) also present dynamical analyses in which the plane of the Kuiper belt is determined. There are two distinct groupings of KBOs as a function of inclination with respect to this plane: the "Core," a dense concentration of objects at low inclination, and the "Halo," a less dense population extending to higher inclinations. Here we investigate KBO colors in the context of the results from Elliot et al. (2005), using previously published color data and new observations from the 6.5-m Clay telescope at Las Campanas Observatory.

2. The Core of the Kuiper belt

Data from the Deep Ecliptic Survey (DES, Millis et al., 2002; Elliot et al., 2005), a program that has discovered nearly 500 designated KBOs, have been used to determine that the pole of the mean orbital plane of the Kuiper belt is at right ascension $273.92° \pm 0.62°$ and declination $66.70° \pm 0.20°$ (Elliot et al., 2005). A plot of KBO orbital poles in right ascension–declination coordinates (Fig. 1) shows the Core and Halo regions with respect to this pole. The Core KBOs are represented by a dense concentration in object poles located within a few degrees of the pole of the Kuiper belt plane, beyond which the Halo objects have a shallower, broader distribution. Although there is no distinct boundary, the unbiased inclination distribution (Figs. 18 and 20 in Elliot et al., 2005) suggests that objects having inclinations with respect to the Kuiper belt plane, i_K, less than $\sim 4.6°$ constitute the Core region, while the Halo distribution extends to $i_K \approx 35°$. This Core boundary represents all objects having inclinations less than the full width at half-maximum of the unbiased inclination distribution divided by $\sin i_K$, rather than the more conservative Core concentration that is distinguished in Fig. 19 of Elliot et al. (2005). The Core and Halo groupings are similar,

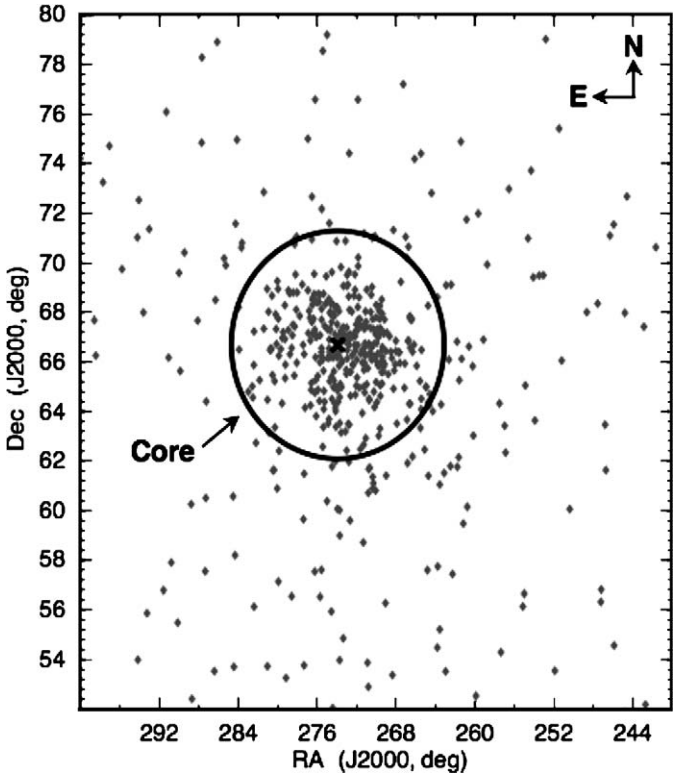

Fig. 1. Orbital poles of KBOs, displayed in right ascension–declination coordinates. Poles are plotted for the 640 provisionally designated KBOs that have errors in pole position less than 0.5°, using orbital elements from the Lowell Observatory database (Buie et al., 2003) on 2005 October 14. The × represents the pole position of the measured Kuiper belt plane (RA = 273.92° and Dec. = 66.70°, Elliot et al., 2005). There is clearly a dense grouping of "Core" objects having poles within a few degrees of the pole of the Kuiper belt plane, beyond which there is a shallower, broader "Halo" of objects. The black circle encompasses objects in the Core sample, those having inclinations $< 4.6°$ with respect to the Kuiper belt plane. For reference, the pole of the invariable plane is approximately 0.3° from the pole of the Kuiper belt plane, at a position angle of 283° (RA = 273.85° and Dec. = 66.99°). This figure is adapted from Elliot et al. (2005).

but not identical to, the dynamically "hot" and "cold" populations discussed by others (e.g., Levison and Stern, 2001; Brown, 2001).

Constraining the Core sample to be provisionally designated KBOs having (i) errors in inclination with respect to the ecliptic $\leqslant 0.05°$ and (ii) inclinations with respect to the Kuiper belt plane $i_K < 4.6°$ results in 307 objects. These objects were selected using the Lowell Observatory database (Buie et al., 2003) as of 2005 October 14. We do not expect that the Core and Halo distributions have abrupt boundaries; therefore, there may be some object overlap between these groupings as we have defined them. Nonetheless, the Core sample contains some objects with extreme dynamical properties: approximately 8% (24) of the Core objects have semimajor axes $a > 50$ AU, 19% (58) have orbital eccentricities $e > 0.2$, and 40% (122) have perihelion distances $q < 40$ AU. In terms of dynamical classifications, the numbers of Classical, Scattered, and Resonant KBOs (using the criteria from Elliot et al., 2005) are 208:5:47, with the remaining 47 objects unclassified due to errors in the orbital elements being too large.

3. Color data

To investigate physical properties of KBOs, we turn to the object colors. The largest compilation of published KBO color data is the Minor Bodies of the Outer Solar System database (MBOSS, Hainaut and Delsanti, 2002). We use the database as of its update on 2005 September 26, when it contained both $B-V$ and $V-R$ color indices for 135 objects that are considered to be KBOs by Elliot et al. (2005). These data represent the average of individual KBO color measurements: while each of the individual measurements is taken as part of a sequence, the compiled colors are the result of non-simultaneous observations. Using the MBOSS database, we found that many of the objects in the Core sample are red. To test this trend, we observed 11 KBOs in the Core region. Only 14% (44 of 307) of the Core objects have $B-V$ and $V-R$ color indices in the MBOSS database, and our observations add 9 objects to the sample. Two of our observed objects overlap published data and serve as a consistency check.

KBO color data were obtained with the Raymond and Beverly Sackler Magellan Instant Camera (MagIC; http://occult.mit.edu/instrumentation/magic) on the 6.5-m Clay telescope at Las Campanas Observatory. MagIC is a SITe 2048 × 2048 pixel CCD camera with a 0.069 arcsec pixel^{-1} plate scale (2.35 × 2.35 arcmin field of view), providing excellent resolution for imaging KBOs. Data were taken during three separate observing runs during 2004 (see dates in Table 1). The seeing ranged from 0.4 to 2.0 arcsec, and the average seeing for the KBO observations was 0.9 arcsec. Observations were made in consecutive image sequences, using Sloan g', r', and i' filters. As a consistency check, the sequences began and ended with observations in r'. The Sloan filters were chosen because they exclude strong night sky lines, the wavelength passbands do not overlap, and their high throughput allows for efficient detection of faint objects (Fukugita et al., 1996). Details on the exposure sequences, including exposure times and signal-to-noise ratios, are listed in Table 1.

To measure magnitudes, we performed aperture photometry on standard stars and KBOs using the PHOT task in the IRAF DIGIPHOT package. While large apertures are necessary to capture light from stars, KBOs are so faint that the background sky noise in such an aperture is sizeable relative to the object signal. Thus we employed the technique of aperture correction (e.g., Barucci et al., 2000), where a small aperture was applied to measure the instrumental magnitude of each KBO and a correction was made using the ratio of the small aperture to a large aperture for bright stars in the frame. We used the average of three bright stars in each frame for aperture correction. The small aperture radius was selected to be a few pixels larger than the full-width at half maximum (FWHM) of the imaged KBOs on each night (∼13 pixel radius, 1.8 arcsec diameter) and the large aperture radius was selected to be three times the FWHM of the imaged standard stars (∼30 pixel radius, 4.1 arcsec diameter). The background signal was calculated from an annulus having an inner radius four times the FWHM of the standard stars, with a radial extent of 10 pixels. The possibility of faint stars or galaxies in the sky background annulus was accounted for in the IRAF fitting routine by the rejection of pixels at the 3σ-level. Extinction coefficients were derived from the standard star observations and used to calibrate KBO magnitudes.

The errors in the calibrated KBO magnitudes were calculated for each frame by combining the instrumental errors with the errors in the derivation of extinction coefficients:

$$\sigma_{\text{mag}} = \sqrt{\sigma_{\text{mi}}^2 + \sigma_{m_0}^2 + X^2\sigma_k^2 + 2\rho X\sigma_{m_0}\sigma_k}, \quad (1)$$

where σ_{mi} is the error in the instrumental KBO magnitude (which includes photon noise from the object and sky), σ_k and σ_{m_0} are errors in the extinction parameters (where k and m_0 are the slope and intercept of the extinction fit, respectively), ρ is the correlation coefficient between the extinction parameters, and X is the airmass. The dominant source of error was σ_{mi}. Other error sources, such as centroiding the object, variation in the stars used for aperture correction, scintillation noise, read

Table 1
Observed Core Kuiper belt objects

Object	Obs. date (UT)[a]	Obs. filter sequence	Exp. time (s)			Avg. SNR per frame			g' (mag)[b]	r' (mag)[b]	i' (mag)[b]
			g'	r'	i'	g'	r'	i'			
$2001KG_{76}$	1	$2r'$-$3i'$-$4g'$-$2r'$	180	120	80	10	17	13	23.71 ± 0.05	22.80 ± 0.03	22.30 ± 0.05
$2002GP_{32}$	1	$2r'$-$4i'$-$4g'$-$2r'$	60	60	60	22	33	25	22.26 ± 0.02	21.74 ± 0.02	21.52 ± 0.02
$2002GZ_{31}$	1	$2r'$-$4i'$-$4g'$-$2r'$	180	120	60	15	22	14	23.35 ± 0.04	22.62 ± 0.02	22.11 ± 0.04
$2003FF_{128}$	1	$2r'$-$4i'$-$4g'$-$2r'$	60	60	60	14	28	25	22.72 ± 0.04	21.88 ± 0.02	21.48 ± 0.02
88268	1	$2r'$-$3i'$-$4g'$-$2r'$	120	120	80	10	18	15	23.48 ± 0.05	22.67 ± 0.03	22.15 ± 0.04
$1999HS_{11}$	2	$2r'$-$4i'$-$4g'$-$2r'$	360	240	180	9	13	11	23.71 ± 0.06	22.78 ± 0.04	22.27 ± 0.05
66652	3	$2r'$-$4i'$-$4g'$-$2r'$	60	60	60	14	23	23	22.19 ± 0.04	21.54 ± 0.02	21.10 ± 0.02
$2001QY_{297}$	3 & 4[c]	$2r'$-$4i'$-$4g'$-$2r'$ $1r'$-$4i'$-$6g'$-$4r'$	60 90	60 90	60 90	14	21	19	22.70 ± 0.02	21.97 ± 0.02	21.55 ± 0.02
$1999RX_{215}$	4	$2r'$-$4i'$-$5g'$-$2r'$	360	240	240	13	15	12	23.95 ± 0.04	23.15 ± 0.04	22.77 ± 0.05
$2000QC_{226}$	4	$2r'$-$4i'$-$4g'$-$2r'$	300	180	180	13	17	17	23.83 ± 0.04	22.97 ± 0.03	22.47 ± 0.03
$2002VD_{131}$	5	$2r'$-$3i'$-$3g'$-$2r'$	300	180	180	28	28	18	23.45 ± 0.02	22.76 ± 0.02	22.67 ± 0.04

[a] Observation date key: 1–25 May 2004, 2–26 May 2004, 3–22 Aug. 2004, 4–11 Sept. 2004, 5–13 Sept. 2004.

[b] Filter characteristics are: g'—peak = 485 nm and FWHM = 110 nm, r'—peak = 625 nm and FWHM = 150 nm, i'—peak = 775 nm and FWHM = 140 nm.

[c] Represents the combination of observations made on two different dates. Details of these observations, in the format of Table 1, are: $2001QY_{297}$, 3, $2r'$-$4i'$-$4g'$-$2r'$, 60, 60, 60, 12, 18, 18, 22.30 ± 0.04, 21.90 ± 0.03, 21.47 ± 0.03 and $2001QY_{297}$, 4, $1r'$-$4i'$-$6g'$-$4r'$, 90, 90, 90, 15, 23, 20, 22.88 ± 0.03, 22.01 ± 0.02, 21.60 ± 0.03.

noise, and the dark current noise, were negligible. The weighted averages of the Sloan magnitudes and errors, over all observations for each KBO, are listed in Table 1.

For comparison with MBOSS colors, the magnitudes were converted from the Sloan system into the Johnson–Cousins system using color transformations provided by the Sloan Digital Sky Survey (Smith et al., 2002). However, the Smith et al. (2002) equations for $B–V$ and $V–R$ depend on only two of the Sloan colors, which forces a linear relationship between these color indices. In order to utilize all three measured Sloan colors, we calculated $B–V\,(g', r')$ and $R–I\,(r', i')$ following Smith et al. (2002), then employed the polynomial relation of Caldwell et al. (1993) to convert $R–I$ to $V–R$. We note that these transformation equations were derived from stellar data, but are currently our best method to convert between color systems.

Including our new observations, we have $B–V$ and $V–R$ data for 53 of the 307 presently known objects in the Core sample. These Core objects are listed in Table 2, with their color indices and selected orbital parameters. The errors in the color indices for the objects we observed are the sum in quadrature of the errors in the Sloan magnitudes used in the color conversion. As a check of photometry, we observed two objects that have previously published colors. For 66652, we obtained $B–V = 0.87 \pm 0.04$ (consistent with Doressoundiram et al., 2001), and

Table 2
Core Kuiper belt objects with measured colors (in order of increasing inclination with respect to the Kuiper belt plane)

Object	Dynamical class[a]	i_K (deg)[b]	i (deg)[c]	e[c]	a (AU)[c]	q (AU)[c]	$B–V$ (mag)	$V–R$ (mag)
$2001KG_{76}$[d]	SE	$0.02^{+0.32}_{-0.02}$	1.55	0.34	52.0	34.1	1.12 ± 0.06	0.80 ± 0.06
$2001QY_{297}$[d]	CL	$0.33^{+0.29}_{-0.07}$	1.55	0.09	43.8	40.0	0.94 ± 0.03	0.73 ± 0.03
$2003FF_{128}$[d]	3:2*e*	$0.38^{+0.30}_{-0.25}$	1.91	0.22	39.8	31.0	1.05 ± 0.04	0.71 ± 0.03
85633	CL	$0.39^{+0.30}_{-0.25}$	1.19	0.03	43.5	42.1	1.10 ± 0.08	0.63 ± 0.07
$1998KS_{65}$	CL	$0.40^{+0.30}_{-0.26}$	1.18	0.03	43.7	42.3	1.09 ± 0.04	0.64 ± 0.02
88268[d]	CL	$0.44^{+0.30}_{-0.32}$	1.89	0.02	42.7	41.9	1.03 ± 0.06	0.81 ± 0.05
$2000OJ_{67}$	CL	$0.45^{+0.26}_{-0.19}$	1.11	0.02	42.7	41.8	1.05 ± 0.06	0.67 ± 0.05
$1995WY_2$	CL	$0.51^{+0.26}_{-0.16}$	1.65	0.13	46.5	40.5	1.00 ± 0.21	0.65 ± 0.19
19255	CL	$0.65^{+0.30}_{-0.20}$	1.49	0.04	42.7	41.2	1.01 ± 0.06	0.66 ± 0.06
$1999RX_{215}$[d]	CL	$0.67^{+0.26}_{-0.23}$	0.89	0.14	46.8	40.2	1.02 ± 0.05	0.69 ± 0.06
$2002GZ_3$[d]	SE	$0.68^{+0.32}_{-0.30}$	1.05	0.24	50.8	38.4	0.94 ± 0.04	0.81 ± 0.05
$2002GP_{32}$[d,e]	5:2*e*[3]	$0.74^{+0.29}_{-0.19}$	1.56	0.43	56.0	32.0	0.72 ± 0.03	0.47 ± 0.03
$2002VD_{131}$[d,e]	CL	$0.75^{+0.29}_{-0.27}$	0.85	0.06	44.9	42.2	0.90 ± 0.03	0.31 ± 0.04
$1999OM_4$	CL	$0.75^{+0.29}_{-0.32}$	2.08	0.12	46.0	40.5	1.14 ± 0.14	0.60 ± 0.10
$1998WX_{24}$	CL	$0.98^{+0.32}_{-0.30}$	0.92	0.04	43.2	41.3	1.09 ± 0.05	0.70 ± 0.05
66652[d]	CL	$1.02^{+0.27}_{-0.26}$	0.56	0.09	43.7	39.8	0.87 ± 0.04	0.74 ± 0.03
$1999HS_{11}$[d]	CL	$1.09^{+0.30}_{-0.28}$	2.60	0.02	44.4	43.4	1.15 ± 0.07	0.81 ± 0.06
$2000CL_{104}$	CL	$1.09^{+0.32}_{-0.28}$	1.24	0.08	44.7	41.2	1.22 ± 0.17	0.66 ± 0.12
$2000QC_{226}$[d]	CL	$1.11^{+0.28}_{-0.23}$	2.66	0.05	44.0	41.7	1.08 ± 0.05	0.80 ± 0.04
52747[e]	CL	$1.14^{+0.29}_{-0.28}$	0.54	0.06	44.6	41.9	0.93 ± 0.09	0.62 ± 0.05
$1999OE_4$	CL	$1.23^{+0.23}_{-0.25}$	2.15	0.04	45.2	43.3	1.10 ± 0.24	0.57 ± 0.16
$1999RE_{215}$	CL	$1.30^{+0.32}_{-0.28}$	1.35	0.11	44.9	40.0	1.00 ± 0.13	0.70 ± 0.07
53311	CL	$1.33^{+0.28}_{-0.27}$	0.37	0.06	44.4	41.6	1.36 ± 0.16	0.67 ± 0.23
$1994ES_2$	CL	$1.34^{+0.32}_{-0.30}$	1.06	0.12	46.1	40.7	0.71 ± 0.15	0.94 ± 0.15
$1999CM_{119}$	CL	$1.42^{+0.30}_{-0.32}$	2.74	0.09	44.1	40.0	0.90 ± 0.19	0.88 ± 0.26
$2001KD_{77}$	3:2*e*	$1.52^{+0.23}_{-0.23}$	2.25	0.12	39.7	35.0	1.12 ± 0.05	0.64 ± 0.05
66452	CL	$1.72^{+0.25}_{-0.28}$	2.66	0.07	44.9	41.9	1.03 ± 0.11	0.67 ± 0.08
24978	CL	$1.73^{+0.23}_{-0.23}$	2.39	0.05	43.6	41.3	1.11 ± 0.03	0.71 ± 0.03
48639[e]	SE	$1.80^{+0.25}_{-0.25}$	0.24	0.23	52.2	40.0	0.83 ± 0.19	0.55 ± 0.16
$1999HR_{11}$[e]	CL	$1.82^{+0.30}_{-0.30}$	3.30	0.04	44.0	42.2	0.92 ± 0.12	0.53 ± 0.10
58534	CL	$1.87^{+0.27}_{-0.30}$	2.90	0.12	45.5	39.9	0.99 ± 0.13	0.73 ± 0.12
33340[e]	3:2*e*	$1.89^{+0.28}_{-0.32}$	3.04	0.25	39.2	29.3	0.93 ± 0.06	0.57 ± 0.05
$1994EV_3$	CL	$2.01^{+0.32}_{-0.28}$	1.65	0.04	43.2	41.6	1.17 ± 0.17	0.57 ± 0.13
$1998KG_{62}$	CL	$2.07^{+0.29}_{-0.29}$	0.79	0.05	43.3	41.1	1.04 ± 0.11	0.58 ± 0.08
$1998WV_{24}$[e]	CL	$2.12^{+0.32}_{-0.30}$	1.52	0.04	38.9	37.4	0.77 ± 0.01	0.50 ± 0.03

(*continued on next page*)

Table 2 (*continued*)

Object	Dynamical class[a]	i_K (deg)[b]	i (deg)[c]	e[c]	a (AU)[c]	q (AU)[c]	$B-V$ (mag)	$V-R$ (mag)
$2000FS_{53}$	CL	$2.15\pm^{0.31}_{0.25}$	2.08	0.04	43.4	41.7	1.09 ± 0.11	0.70 ± 0.08
$1999CO_{153}$	CL	$2.36\pm^{0.24}_{0.25}$	0.80	0.09	43.9	40.0	1.03 ± 0.10	0.91 ± 0.13
33001	CL	$2.41\pm^{0.32}_{0.30}$	1.45	0.04	43.6	41.9	1.13 ± 0.11	0.65 ± 0.06
60454	CL	$2.53\pm^{0.29}_{0.29}$	1.16	0.09	44.6	40.7	1.02 ± 0.09	0.68 ± 0.06
$1996TK_{66}$	CL	$2.66\pm^{0.22}_{0.26}$	3.32	0.02	42.5	41.8	0.99 ± 0.06	0.68 ± 0.07
$2000CL_{105}$[e]	CL	$2.72\pm^{0.30}_{0.30}$	4.18	0.04	43.2	41.3	1.11 ± 0.08	0.41 ± 0.12
15788[e]	3:2*e*	$2.73\pm^{0.32}_{0.30}$	1.94	0.32	39.2	26.7	0.80 ± 0.07	0.48 ± 0.08
$1999OJ_4$	CL	$2.78\pm^{0.30}_{0.32}$	4.00	0.02	38.0	37.1	1.10 ± 0.16	0.67 ± 0.07
$1999HV_{11}$	CL	$2.84\pm^{0.25}_{0.21}$	3.15	0.02	43.2	42.3	1.11 ± 0.06	0.59 ± 0.02
15760[e]	CL	$2.85\pm^{0.32}_{0.29}$	2.19	0.07	43.7	40.9	0.84 ± 0.15	0.71 ± 0.10
15810	3:2*e*	$2.99\pm^{0.25}_{0.29}$	3.81	0.12	39.5	34.7	1.01 ± 0.18	0.66 ± 0.12
80806	CL	$3.02\pm^{0.24}_{0.28}$	3.76	0.06	42.3	39.6	1.14 ± 0.23	0.84 ± 0.33
$2001KP_{77}$	7:4e^3	$3.27\pm^{0.28}_{0.21}$	3.31	0.18	43.9	36.0	1.54 ± 0.24	0.70 ± 0.12
$1999HT_{11}$	7:4e^3	$3.52\pm^{0.28}_{0.27}$	5.05	0.12	44.0	38.9	1.14 ± 0.14	0.69 ± 0.17
16684	CL	$3.55\pm^{0.26}_{0.20}$	3.73	0.05	44.4	42.0	1.13 ± 0.07	0.74 ± 0.10
1993RO[e]	3:2*e*	$3.61\pm^{0.27}_{0.20}$	3.72	0.19	39.0	31.5	0.93 ± 0.16	0.58 ± 0.13
79360	CL	$3.70\pm^{0.28}_{0.29}$	2.24	0.01	44.0	43.3	1.05 ± 0.08	0.67 ± 0.05
$1999CJ_{119}$	CL	$4.55\pm^{0.30}_{0.30}$	3.20	0.07	45.5	42.3	1.38 ± 0.18	0.69 ± 0.28

[a] Classification based on the system described in Elliot et al. (2005): Classical—CL, Scattered Extended—SE, Resonant—(3:2*e*, 7:4e^3, and 5:2e^3).
[b] Errors in inclination with respect to the Kuiper belt plane are dominated by the error in the measured pole of the plane (as listed in Table 13, Elliot et al., 2005).
[c] Orbital elements are from the Lowell Observatory database (Buie et al., 2003) on 2005 October 14. The errors on i, e, a, and q are smaller than the least significant digit, with the exception of object $1999CM_{119}$ which has $\sigma_i = 0.01$, $\sigma_e = 0.10$, and $\sigma_q \approx \sigma_a = 0.8$.
[d] Objects with colors measured in this work. Details of the observations and the measured Sloan magnitudes are listed in Table 1. Color indices for objects without this superscript were obtained from http://www.sc.eso.org/~MBOSS, as of its update on 2005 September 26.
[e] Neutral objects, with $B-R < 1.56$.

$V-R = 0.74 \pm 0.04$ (consistent with Delsanti et al., 2001). For $1999HS_{11}$, we obtained $B-V = 1.15 \pm 0.07$ (consistent with Doressoundiram et al., 2001; Tegler and Romanishin, 2003; Peixinho et al., 2004), and $V-R = 0.81 \pm 0.06$ (consistent with Doressoundiram et al., 2001; inconsistent with Tegler and Romanishin, 2003, by 0.09 mag; inconsistent with Peixinho et al., 2004, by 0.18 mag).

4. Analysis

A color–color plot for all KBOs with $B-V$ and $V-R$ values (comprised of the MBOSS database and this work) is shown in Fig. 2a. Error bars are not plotted for visual clarity. The objects are distinguished by dynamical classification, as determined following Elliot et al. (2005). We use the median of the objects in this plot ($B-R = 1.56$) to differentiate KBOs into two color groupings: red ($B-R > 1.56$) and neutral ($B-R < 1.56$). We select the median as our color boundary because it is a more robust estimator of the central value of the distribution than the mean. A few trends are apparent in Fig. 2a: (i) Classical objects are generally red, (ii) Scattered Near objects are generally neutral, and (iii) Scattered Extended and Resonant objects are fairly evenly distributed across the range of colors.

In Fig. 2b, the Resonant objects are plotted exclusively, with distinct resonances denoted by different plot symbols. From this figure, we see that the 3:2 objects constitute the majority of Resonant objects for which we have colors. Thus the range of KBO colors in the 3:2 resonance dominates the group characteristic. Objects in the 5:2 resonance tend to be neutral, while objects in all other resonances (excluding the 3:2) tend to be red. In particular, one of the two objects in the 7:4 resonance is the reddest KBO for which we have $B-V$ and $V-R$ color indices.

A color–color plot of the Core objects is shown in Fig. 3a. Dynamical classifications of these objects are represented by the same symbols as Fig. 2a. Open boxes encompass the data points for KBOs with colors measured in this work, while all other colors are from the MBOSS database. The diagonal line demarks the color boundary between red and neutral objects. In Fig. 3a, it is clear that the majority of the Core objects are red. Displaying the error bars causes the plot to be somewhat cluttered, but they are necessary to illustrate the rather large uncertainties on some KBO color indices

To further investigate the trend seen in Fig. 3a of the Core objects being red, we reduce ambiguity near the color boundary by selecting the subset of Core objects with $B-V$ and $V-R$ color index errors less than 0.1 mag. In addition, it is possible that the compositions and environmental histories of Resonant objects differ from the other KBOs, since they formed in the inner part of the Kuiper belt and were subsequently captured into resonances by Neptune as it migrated outward (Malhotra, 1996; Jewitt and Luu, 2001). The resonance sweeping process could have affected the colors of the Resonant objects; therefore, we

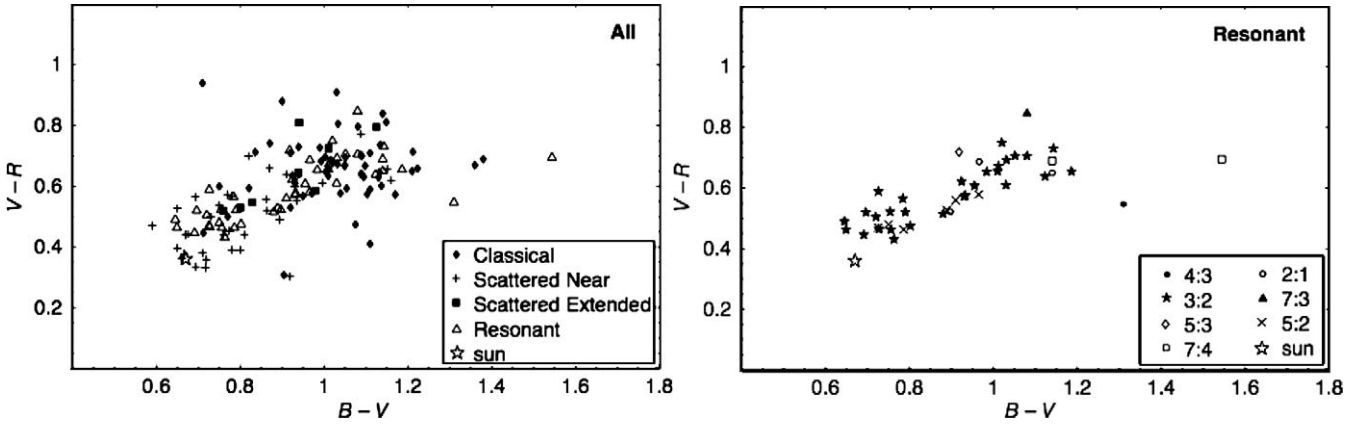

(a) (b)

Fig. 2. Color–color plots of KBOs, distinguished by dynamical class. The data represent objects having $B–V$ and $V–R$ color indices from this work and in the MBOSS database (Hainaut and Delsanti, 2002). For clarity, error bars are not plotted and the color of the Sun is plotted as an open star. (a) Colors of all objects, with different symbols distinguishing between the four dynamical classifications from Elliot et al. (2005). The median $B–R$ for these objects is 1.56. With respect to the overall sample, Classical objects tend to be red ($B–R > 1.56$), Scattered Near objects tend to be neutral ($B–R < 1.56$), and Scattered Extended and Resonant objects are fairly evenly distributed (see Table 3 for quantification). (b) Colors of the Resonant objects from (a), with symbols distinguishing different resonances. Objects in the 3:2 resonance have colors spanning those of all KBOs, while the objects in the 5:2 resonance are primarily neutral. In the remaining resonances, the objects are predominantly red. One of the two objects in the 7:4 resonance is remarkably red relative to all other KBOs.

choose to focus on objects that are non-Resonant. A color–color plot for this refined subset, the non-Resonant Core objects with low color error, is shown in Fig. 3b. The overwhelming majority of these objects are red.

While Figs. 2 and 3 provide visual representation of KBO colors as a function of dynamical grouping, we require statistical methods to determine the significance of the observed trends. All of the dynamical samples represented in these plots are listed in Table 3, and we have included the Halo ($i_K > 4.6°$) as an additional grouping. First, we calculate the mean and median $B–R$ for each sample, the standard deviation of the mean, and the percent of objects that are red and neutral (relative to the median $B–R$ of All objects). The mean $B–R$ values for many samples, particularly Classical, Scattered Near, non-Resonant subsets of the Core and Halo, and some of the resonances, are a significant number of standard deviations from the mean $B–R$ of All objects. This comparison draws attention to the samples that may be distinctive, but it does not say anything about color distribution or statistical significance.

Next, we look at the percentages of red and neutral objects in each sample to provide a numerical basis for the color trends seen in Figs. 2 and 3: 76% of Classical objects are red, 88% of Scattered Near objects are neutral, 79% of Core objects are red, and 86% of non-Resonant, low-color-error Core objects are red. The highest percentage of red KBOs (for samples containing >2 objects) is found in the grouping of non-Resonant, low-color-error Core objects, which are shown in Fig. 3b. These percentages provide a rough characterization of the color distributions, but they still do not represent the statistical significance of the groupings.

We can begin to gain an understanding of the significance of the color differences by comparing the mean $B–R$ for each sample to that of a complementary sample, using Student's t-test (Press et al., 1992). For most samples, the complementary grouping is the remaining KBOs; however, subsets of samples must be compared to subsets of the remaining objects. Thus the samples for specific resonances are compared to all other Resonant objects, the non-Resonant subset of the Core is compared to the Halo, and the non-Resonant subset of the Halo is compared to the Core. For completeness, we also compare the non-Resonant Core to the non-Resonant Halo. Although we use the median $B–R$ to discriminate between colors, Student's t-test employs the mean as a first-order measurement of the difference between the samples. This test returns the probability that t (a measure of the standard error of the difference of the means) could be equal to or larger than the observed value by chance, for distributions with equal means. Small probabilities imply that the observed difference between the means is significant. Based on the results of an F-test, we use the unequal variance version of Student's t-test for the samples Classical, 3:2, 2:1, 5:2, Core, Halo, and the non-Resonant subsets of the Core and Halo (Press et al., 1992). Assuming a two-tailed probability distribution, the t-test probabilities for each of our dynamical samples are listed in Table 3. The samples having a significantly different mean $B–R$ from the remaining KBOs (to the >99.99% significance level) are Classical, Scattered Near, Core, Halo, and the non-Resonant, low-color-error subsets of the Core and Halo.

Since the comparisons in this test are being made between each sample and a complementary group of the remaining KBOs, significance levels are identical for samples that form the entire set when combined: Core and Halo, Resonant and non-Resonant. This correlation reveals one of the difficulties in determining the significance of the colors in each dynamical sample. If the comparison sample contains a grouping of objects having unusual colors, it can skew the results. Nonetheless, until we have determined specific color groupings and provided adequate reasons for their elimination from comparison samples, this method is the most straightforward.

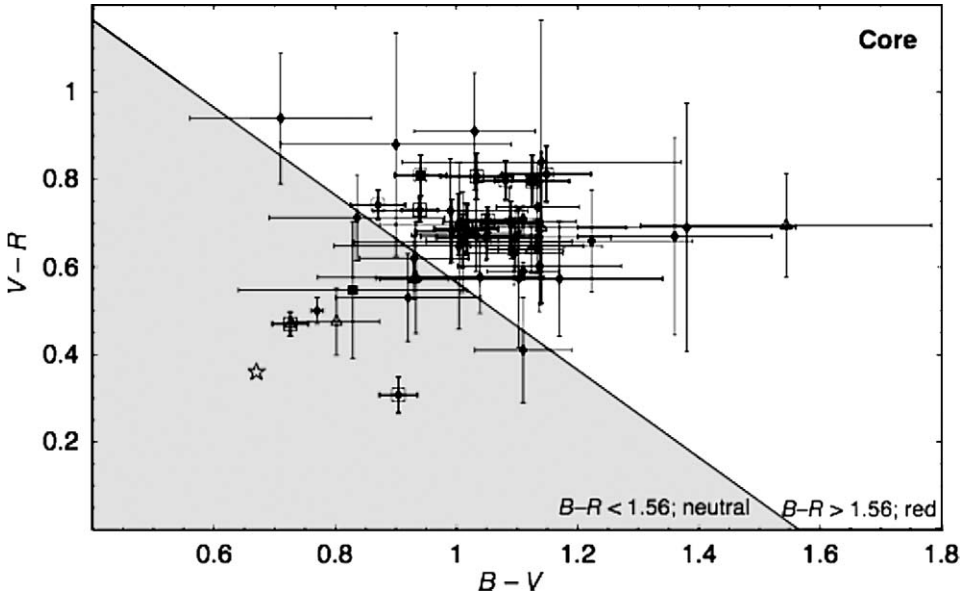

Fig. 3. Color–color plots of Core KBOs ($i_K < 4.6°$). Classes are distinguished by the same symbols as Fig. 2a. Data points for objects observed in this work are encompassed by open squares to distinguish them from MBOSS data (Hainaut and Delsanti, 2002). For reference, the color of the Sun is plotted as an open star. The white regions of the plots contain red objects ($B–R > 1.56$) and the shaded regions contain neutral objects ($B–R < 1.56$). (a) Color indices with error bars for all KBOs in the Core. These objects are predominantly red, with 42 out of 53 objects having $B–R > 1.56$. (b) A subset of the data shown in (a), excluding Resonant KBOs and objects having $B–V$ or $V–R$ error greater than 0.1 mag. The objects in this subset form a distinctive red cluster, with just a few outliers. The two objects having colors well outside of the cluster are both Classical: $1998WV_{24}$ and $2002VD_{131}$.

Student's t-test assumes that the samples are normally distributed, which is not necessarily the case for the colors of KBOs with respect to their dynamical groupings. Thus we also employ the Kolmogorov–Smirnov (K–S) test, which makes no assumptions about the distribution of each sample (Press et al., 1992). The 1-D K–S test determines if two samples are significantly different by evaluating the probability that a random distribution would result in a larger difference between the samples than that observed. To perform the K–S test, we compare the piecewise continuous functions of the cumulative $B–R$ distribution for each sample and its complementary grouping. The results of the K–S test are listed in Table 3. This test is particularly useful because it quantifies the significance of the colors of objects in specific resonances, even though these samples tend to be very small. Specific resonances in which objects exhibit the greatest color difference from the remaining Resonant objects are the 3:2, 7:4 and 5:2 (significance levels of 98.7%, 97.1%, and 96.3%, respectively). The K–S test also confirms that the samples identified by the Student's t-test have significantly different distributions (>99.99% significance level) than the objects to which they are being compared. The differences in the color distributions for these samples are apparent

Table 3
Kuiper belt object colors by dynamical grouping

Sample[a]	No. KBOs	Median $B-R$ (mag)	Mean $B-R$ (mag)	Standard deviation of mean, σ (mag)	Red percent of sample $B-R > 1.56$	Neutral percent of sample $B-R < 1.56$	% Sig. level from Student's t-test[b] $(1 - A(t \mid \nu))$	% Sig. level from K–S test[c] (D)
All	144	1.56	1.54	0.02	50%	50%	–	–
Classical	58	1.70	1.68	0.02	76%	24%	>99.99 (1×10^{-9})	>99.99 (0.50)
Scattered Near	34	1.25	1.31	0.04	12%	88%	>99.99 (1×10^{-9})	>99.99 (0.55)
Scattered Extended	8	1.57	1.57	0.08	63%	38%	26.4 (0.74)	41.4 (0.26)
All Non-Resonant	101	1.59	1.55	0.03	53%	47%	50.7 (0.49)	99.3 (0.17)
Resonant	43	1.51	1.51	0.04	42%	58%	50.7 (0.49)	82.6 (0.17)
4:3[d]	1	1.86	1.86	–	100%	0%	–	85.3 (0.93)
3:2	29	1.50	1.47	0.05	45%	55%	87.4 (0.13)	98.7 (0.29)
5:3[d]	1	1.64	1.64	–	100%	0%	–	34.3 (0.60)
7:4	2	2.03	2.03	0.20	100%	0%	99.6 (4×10^{-3})	97.1 (0.90)
2:1	3	1.65	1.62	0.11	67%	33%	59.7 (0.40)	55.27 (0.45)
7:3[d]	1	1.93	1.93	–	100%	0%	–	88.8 (0.98)
5:2	6	1.33	1.35	0.06	17%	83%	97.4 (0.03)	96.3 (0.54)
Core ($i_K < 4.6°$)	53	1.72	1.70	0.03	79%	21%	>99.99 (3×10^{-10})	>99.99 (0.55)
Non-Res. Core[e]	21	1.72	1.70	0.04	86%	14%	>99.99 (3×10^{-6})	>99.99 (0.61)
							>99.99 (2×10^{-6})[f]	>99.99 (0.67)[f]
Halo ($i_K > 4.6°$)	91	1.42	1.44	0.03	34%	66%	>99.99 (3×10^{-10})	>99.99 (0.55)
Non-Res. Halo[e]	36	1.35	1.38	0.04	28%	72%	>99.99 (4×10^{-8})	>99.99 (0.62)
							>99.99 (2×10^{-6})[f]	>99.99 (0.67)[f]

[a] Samples contain KBOs for which there are $B-V$ and $V-R$ colors in this work or the MBOSS database. Classifications are based on the system described in Elliot et al. (2005).

[b] The significance of the variation between the mean $B-R$ of each sample and that of the remaining KBOs, using a two-tailed Student's t-test for samples of unequal variance (Press et al., 1992). For resonant subsamples, the comparison is relative to the other Resonant objects. For the non-Resonant subsamples of the Core and Halo, the comparison is relative to the Halo and Core, respectively. Values in parentheses are the probability of obtaining a t-value equal to or larger than that of the sample by chance, thus low numbers (<0.05) indicate that the means of the samples are significantly different.

[c] The significance of the variation between the cumulative distribution functions of $B-R$ for each sample and that of the remaining KBOs, using a Kolmogorov–Smirnov test (Press et al., 1992). For the Resonant subsamples, the comparison is relative to the other Resonant objects. For the non-Resonant subsamples of the Core and Halo, the comparison is relative to the Halo and Core, respectively. Values in parentheses are D, the absolute value of the maximum difference between the cumulative distribution functions.

[d] Denotes samples that contain too few objects for all of the statistical analyses.

[e] These samples are also limited to objects with $B-V$ and $V-R$ color index errors < 0.1 mag.

[f] The significance of the statistical variation between the sample and the non-Resonant, low-color error subset of the complementary sample: non-Resonant Core is compared to non-Resonant Halo and vice versa.

in Fig. 4, which shows the cumulative distributions of $B-R$ for All, Classical, Scattered Near, and the non-Resonant, low-color-error subsets of the Core and Halo. The color distributions are the most extreme for the samples of Scattered Near (very neutral) and non-Resonant, low-color-error Core (very red).

5. Discussion and conclusions

We find that objects classified as Classical and Scattered Near (using the classification scheme of Elliot et al., 2005) have significant correlation with color. Classical objects tend to be red (76%), while Scattered Near objects are predominantly neutral (88%). Of the dynamical groupings we investigated, the Scattered Near objects contain the highest percentage of neutral bodies.

Analysis of the colors of Resonant objects is limited by small number statistics. However, the trends we observe warrant further investigation. Like previous studies (e.g., Trujillo and Brown, 2002; Peixinho et al., 2004), we find that objects classified as being in the 3:2 resonance span the full range of KBO colors. However, this distribution contrasts with the neutral colors of the 5:2 objects and the redness of the objects in the other resonances. The objects in the 7:4 resonance are remarkably red, with $2001KP_{77}$ being the reddest for which we have colors, $B-R = 2.24 \pm 0.27$ (2.5σ redder than the median $B-R$ of All KBOs). Further exploration of the relationships between color and resonance occupation can shed light on the history of these objects, including testing origin theories of capture, collision, or accretion (Chiang et al., 2003; Chiang and Lithwick, 2005).

We also find that the groupings based on inclination with respect to the Kuiper belt plane, the Core and Halo, are significantly correlated with color. The majority of the Core objects are red (79%) while the Halo objects are slightly more likely to be neutral (66%). When the Core and Halo samples are refined to include only non-Resonant objects with errors in $B-V$ and $V-R$ less than 0.1 mag, the dominant colors of each grouping are even more pronounced. In particular, the non-Resonant, low-color-error Core sample has the highest concentration of red objects (of samples we examined containing >2 objects; 86%).

We do not yet know whether the KBO inclination distribution is continuous or consists of two (or more) discrete populations. Our definitions of Core and Halo assume that there are

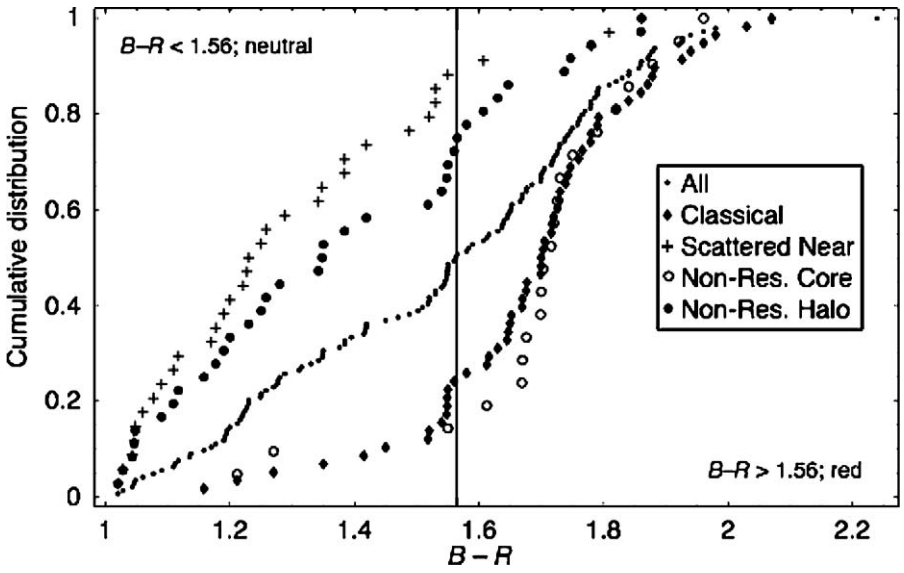

Fig. 4. Cumulative color distributions for select KBO dynamical samples. This plot shows the fraction of objects (from 0 to 1) as a function of increasing $B–R$ for the samples listed in Table 3 that have distinctive color trends. Samples shown are All (for comparison), Classical, Scattered Near, and the non-Resonant, low-color-error subsets of the Core and Halo. Cumulative distributions for the full Core and Halo samples are similar to, but less deviant from the bulk distribution than, these subsets and have not been displayed for clarity. The solid line demarks the red/neutral color boundary. This plot highlights the color trends discussed in the text: the sample of Classical objects tends to be red and the non-Resonant Halo objects tend to be neutral. Of the samples tested, the most extreme color distributions are those of Scattered Near (predominantly neutral) and non-Resonant Core (predominantly red).

two distributions, with no overlap. However, it is more likely that there is no abrupt boundary between these populations. We thus envision that the tails of the Core and Halo may intersect, or that the distributions may even overlie one another. In either case, some objects that we have defined as being in the Core may be more appropriately grouped with the Halo (and vice versa).

We do not yet have a method to distinguish which objects meeting our Core criteria could be part of the Halo. However, using the set of objects from the inclination distribution in Elliot et al. (2005), we find that the densities of non-Resonant KBO orbital poles in an unbiased sample of objects are 2.17 deg^{-2} in the Core and 0.23 deg^{-2} in the densest subset of the Halo ($4.6° < i_K < 9.2°$). Assuming that the Halo is a separate population, which is continuous and underlies the Core, approximately 2 of the 21 non-Resonant Core objects with low color errors shown in Fig. 3b, could be from the Halo. Approximately 72% of these are expected to be neutral in color (Table 3). Therefore, the two clearly neutral objects in the non-Resonant, low-color-error Core sample (Fig. 3b) may be from the Halo. There is a third object in the shaded portion of Fig. 3b, which lies just on the neutral side of our defined color boundary, at $B–R = 1.55$. Further refinement of the error bars on this object, and the choice of color boundary, are required to determine if this object should be considered neutral or red. By taking into consideration the possible overlap between the Core and Halo, we conclude that virtually all of the non-Resonant objects in the Core are red.

While the Core sample is similar to previously noted groupings of red KBOs (Tegler and Romanishin, 2000; Jewitt and Luu, 2001; Trujillo and Brown, 2002; McBride et al., 2003), it has slight, but notable, distinctions: the Core contains objects with $q < 40$ AU and is not limited to objects classified as "classical." Since Classical objects are the primary constituents of the Core (77% of all Core objects and 90% of non-Resonant, low-color-error Core objects), it follows that Classical Core objects are primarily red (85%). However, the few neutral objects in the non-Resonant, low-color-error subset of the Core (Fig. 3b) are (i) Classical and (ii) have orbital parameters well below the inclination and eccentricity boundaries used for classification. This pattern of neutral Core objects being Classical could be a statistical effect, due to the predominance of Classical objects in the sample. Alternatively, these objects may represent yet another grouping of objects that has distinctive characteristics.

Interestingly, our dynamically-defined Core sample is most similar to the grouping found by Peixinho et al. (2004) solely from color analysis. By measuring the inclination cutoff below which the color variance was smaller than that above, Peixinho et al. (2004) noted a red cluster of classical objects having inclination < 4.5° (where "classical" is defined as objects in "quasi-circular orbits with semi-major axis between 35 and 48 AU"). While not explicitly stated, we assume their KBO inclinations are with respect to the ecliptic, which is a difference of up to 1.56° from inclinations referenced to the Kuiper belt plane. Nonetheless, it is noteworthy that the Peixinho et al. (2004) cutoff is similar to our inclination boundary of $i_K < 4.6°$. We think that our characterization of the Core serves to more precisely define this red grouping, since (i) we do not restrict the objects by dynamical classification, (ii) our analysis is with respect to the Kuiper belt plane, and (iii) the inclination limit by which we define the Core is based on fits to the full KBO inclination distribution (Elliot et al., 2005), rather than those objects with measured colors.

We present two explanations for the predominant redness of the Core KBOs. First, objects in the Core may have inher-

ently different surface compositions from objects in the Halo. However, there is no clear reason why these objects should have different compositions or how they would have maintained this difference throughout their history. A second explanation for the redness of the Core objects is that they may represent a particularly unperturbed, relic grouping. KBO colors have been modeled as the balance between reddening processes, such as surface irradiation, and "bluing" processes like collisional resurfacing and cometary activity (Jewitt and Luu, 2001; Luu and Jewitt, 1996; Delsanti et al., 2004). In this view, objects with low inclinations may appear redder because they formed farther out in the Solar System, remained relatively unperturbed by Neptune, and were able to retain an irradiated crust (Trujillo and Brown, 2002; Tegler et al., 2003; Gomes, 2003). In contrast, KBOs that have undergone collisions have younger, more neutral materials on the surface. Some models, however, predict no correlation between inclination and color (Delsanti et al., 2004), implying that additional color factors may be at work.

Since we currently have $B–V$ and $V–R$ colors for less than 15% of provisionally designated KBOs, the shapes of the color distributions for our dynamical samples could change with additional data. Analysis of the colors of the Resonant objects will particularly benefit from larger-number statistics. Future observations will also be able to place more stringent constraints on the distinctions between the Core and Halo and help clarify the relationship between Core membership and red color.

Acknowledgments

We thank K. Clancy, S. Kern, P. Schechter, and A. Vaz for their help observing at Las Campanas and telescope operators V. Meriño and G. Martin. We also appreciate detailed suggestions from an anonymous reviewer and comments from Mike Brown. Partial support for this work comes from NASA's Planetary Astronomy Program (Grants NAG5-10444 and NNG04-GF25G) and NSF's Division of Astronomical Sciences (Grant AST-0406493).

References

Barucci, M.A., Romon, J., Doressoundiram, A., Tholen, D.J., 2000. Compositional surface diversity in the trans-neptunian objects. Astrophys. J. 120, 496–500.

Barucci, M.A., Fulchignoni, M., Birlan, M., Doressoundiram, A., Romon, J., Boehnhardt, H., 2001. Analysis of trans-neptunian and centaur colours: Continuous trend or grouping? Astron. Astrophys. 371, 1150–1154.

Boehnhardt, H., Tozzi, G.P., Birkle, K., Hainaut, O., Sekiguchi, T., Vair, M., Watanabe, J., Rupprecht, G., T.F.I. Team, 2001. Visible and near-IR observations of trans-neptunian objects: Results from ESO and Calar Alto telescopes. Astron. Astrophys. 378, 653–667.

Brown, M.E., 2001. The inclination distribution of the Kuiper belt. Astron. J. 121, 2804–2814.

Buie, M.W., Millis, R.L., Wasserman, L.H., Elliot, J.L., Kern, S.D., Clancy, K.B., Chiang, E.I., Jordan, A.B., Meech, K.J., Wagner, R.M., Trilling, D.E., 2003. Procedures, resources and selected results of the Deep Ecliptic Survey. Earth Moon Planets 92, 113–124.

Caldwell, J.A.R., Cousins, A.W.J., Ahlers, C.C., van Wamelen, P., Maritz, E.J., 1993. Statistical relations between the photometric colours of common types of stars in the UBV(RI)c, JHK and uvby systems. SAAO Circ. 15.

Chiang, E.I., Lithwick, Y., 2005. Neptune Trojans as a test bed for planet formation. Astrophys. J. 628, 520–532.

Chiang, E.I., Jordan, A.B., Millis, R.L., Buie, M.W., Wasserman, L.H., Elliot, J.L., Kern, S.D., Trilling, D.E., Meech, K.J., Wagner, R.M., 2003. Resonance occupation in the Kuiper belt: Case examples of the 5:2 and 1:1 resonances. Astron. J. 126, 430–443.

Delsanti, A., Boehnhardt, H., Barrera, L., Meech, K.J., Sekiguchi, T., Hainaut, O., 2001. BVRI photometry of 27 Kuiper belt objects with ESO/very large telescope. Astron. Astrophys. 380, 347–358.

Delsanti, A., Hainaut, O., Jourdeuil, E., Meech, K.J., Boehnhardt, H., Barrera, L., 2004. Simultaneous visible-near IR photometric study of Kuiper belt object surfaces with the ESO/very large telescopes. Astron. Astrophys. 417, 1145–1158.

Doressoundiram, A., Barucci, M.A., Romon, J., 2001. Multicolor photometry of trans-neptunian objects. Icarus 154, 277–286.

Doressoundiram, A., Peixinho, N., De Bergh, C., Fornasier, S., Thebault, P., Barucci, M.A., Veillet, C., 2002. The color distribution in the Edgeworth–Kuiper belt. Astron. J. 124, 2279–2296.

Edgeworth, K.E., 1949. The origin and evolution of the Solar System. Mon. Not. R. Astron. Soc. 109, 600–609.

Elliot, J.L., Kern, S.D., Clancy, K.B., Gulbis, A.A.S., Millis, R.L., Buie, M.W., Wasserman, L.H., Chiang, E.I., Jordan, A.B., Trilling, D.E., Meech, K.J., 2005. The Deep Ecliptic Survey: A search for Kuiper belt objects and centaurs. II. Dynamical classification, the Kuiper belt plane, and the core population. Astron. J. 129, 1117–1162.

Fukugita, M., Ichikawa, T., Gunn, J.E., Doi, M., Shimasaku, K., Schneider, D.P., 1996. The Sloan digital sky survey photometric system. Astron. J. 111, 1748–1756.

Gomes, R.S., 2003. The common origin of the high inclination TNOs. Earth Moon Planets 92, 29–42.

Green, S.F., McBride, N., O'Ceallaigh, D.R., Fitzsimmons, A., Williams, I.P., Irwin, M.J., 1997. Surface reflectance properties of distant Solar System bodies. Mon. Not. R. Astron. Soc. 290, 186–192.

Hainaut, O., Delsanti, A., 2002. Colors of minor bodies in the outer Solar System. Astron. Astrophys. 389, 641–664.

Jewitt, D., Luu, J., 1993. Slow moving object 1992 QB1: A Kuiper belt candidate. Nature 362, 730–732.

Jewitt, D., Luu, J.X., 2001. Colors and spectra of Kuiper belt objects. Astron. J. 122, 2099–2114.

Kuiper, G.P., 1951. On the origin of the Solar System. In: Hynek, J.A. (Ed.), Astrophysics. McGraw–Hill, New York, pp. 357–424.

Leonard, F.C., 1930. The new planet Pluto. Astron. Soc. Pacific Leaflet 1, 121.

Levison, H.F., Stern, S.A., 2001. On the size dependence of the inclination distribution of the main Kuiper belt. Astron. J. 121, 1730–1735.

Luu, J., Jewitt, D., 1996. Color diversity among the centaurs and Kuiper belt objects. Astron. J. 112, 2310–2318.

Malhotra, R., 1996. The phase space structure near Neptune resonances in the Kuiper belt. Astron. J. 111, 504–516.

McBride, N., Green, S.F., Davies, J.K., Tholen, D.J., Sheppard, S.S., Whiteley, R.J., Hillier, J.K., 2003. Visible and infrared photometry of Kuiper belt objects: Searching for evidence of trends. Icarus 161, 501–510.

Millis, R.L., Buie, M.W., Wasserman, L.H., Elliot, J.L., Kern, S.D., Wagner, R.M., 2002. The Deep Ecliptic Survey: A search for Kuiper Belt objects and centaurs. I. Description of methods and initial results. Astron. J. 123, 2083–2109.

Peixinho, N., Doressoundiram, A., Delsanti, A., Boehnhardt, H., Barucci, M.A., Belskaya, I., 2003. Reopening the TNOs color controversy: Centaurs bimodality and TNOs unimodality. Astron. Astrophys. 410.

Peixinho, N., Boehnhardt, H., Belskaya, I.N., Doressoundiram, A., Barucci, M.A., Delsanti, A., 2004. ESO large program on Centaurs and TNOs: Visible colors—Final results. Icarus 170, 153–166.

Press, W.H., Teukolsky, S.A., Vetterling, W.T., Flannery, B.P., 1992. Numerical Recipes in FORTRAN: The Art of Scientific Computing. Cambridge Univ. Press, Cambridge.

Smith, J.A., Tucker, D.L., Kent, S., Richmond, M.W., Fukugita, M., Ichikawa, T., Ichikawa, S., Jorgensen, A.M., Uomoto, A., Gunn, J.E., Hamabe, M., Watanabe, M., Tolea, A., Henden, A.A., Annis, J., Pier, J.R., McKay, T.A.,

Brinkmann, J., Chen, B., Holtzman, J., Shimasaku, K., York, D.G., 2002. The u′ g′ r′ i′ z′ standard-star system. Astron. J. 123, 2121–2144.

Tegler, S.C., Romanishin, W., 1998. Two distinct populations of Kuiper belt objects. Nature 392, 49–50.

Tegler, S.C., Romanishin, W., 2000. Extremely red Kuiper belt objects in near-circular orbits beyond 40 AU. Nature 407, 979–980.

Tegler, S., Romanishin, W., 2003. Resolution of the Kuiper belt object color controversy: Two distinct color populations. Icarus 161, 181–191.

Tegler, S.C., Romanishin, W., Consolmagno, G.J., 2003. Color patterns in the Kuiper belt: A possible primordial origin. Astrophys. J. 599, L49–L52.

Trujillo, C.A., Brown, M.E., 2002. A correlation between inclination and color in the classical Kuiper belt. Astrophys. J. 566, L125–L128.